Initial Determination of the NOAA-20 VIIRS screen transmittances with both yaw maneuver and regular on-orbit data

Ning Lei, Xiaoxiong Xiong

Ning Lei, Xiaoxiong Xiong, "Initial Determination of the NOAA-20 VIIRS screen transmittances with both yaw maneuver and regular on-orbit data," Proc. SPIE 10781, Earth Observing Missions and Sensors: Development, Implementation, and Characterization V, 107810F (23 October 2018); doi: 10.1117/12.2324529

SPIE.

Event: SPIE Asia-Pacific Remote Sensing, 2018, Honolulu, Hawaii, United States

Initial Determination of the NOAA-20 VIIRS Screen Transmittances with both Yaw Maneuver and Regular On-orbit Data

Ning Lei*[a] and Xiaoxiong Xiong[b]

[a]Science Systems and Applications, Inc., 10210 Greenbelt Road, Suite 600, Lanham, MD 20706 USA;
[b]Sciences and Exploration Directorate, NASA Goddard Space Flight Center, Greenbelt, MD 20771 USA
* **Corresponding author:** ning.lei@ssaihq.com, tel: +1-301-867-2066

ABSTRACT

One of the scientific instruments aboard the NOAA-20 satellite is the Visible Infrared Imaging Radiometer Suite (VIIRS). The VIIRS regularly performs on-orbit radiometric calibration of its reflective solar bands, primarily through observations of an onboard sunlit solar diffuser (SD). The incident sunlight passes through an attenuation screen (the SD screen) and scatters off the SD to provide a radiance source for the calibration. The on-orbit change of the SD bidirectional reflectance distribution function (BRDF), denoted as the H-factor, is determined by an onboard solar diffuser stability monitor (SDSM). The eight SDSM detectors observe the sun through another attenuation screen (the SDSM screen) and the sunlit SD almost at the same time to measures the SD BRDF change. The products of the SD screen transmittance and the BRDF at t=0 and the SDSM screen transmittance were measured prelaunch. Large undulations in the H-factor were seen when using the prelaunch screen transmittances. Fifteen on-orbit yaw maneuvers were performed to validate and to further characterize the screens. Although significantly improved, the H-factor from the yaw maneuver data determined screen transmittance still has undulations as large as about 0.7-0.8%, revealing that the angular step size of the yaw maneuvers is too large. In this paper, we add regular on-orbit data to the yaw maneuver data to further improve the relative products and the relative SDSM screen transmittance. The H-factor time series derived from the newly determined screen transmittance is much smoother than that derived from using only the yaw maneuver data and thus improves considerably the radiometric calibration accuracy.

Index Terms: N20 VIIRS, radiometric calibration, screens, SDSM screen, SD screen

1. INTRODUCTION

The second Visible Infrared Imaging Radiometer Suite (VIIRS) is on the NOAA-20 (N20) satellite launched on November 18, 2017. The N20 satellite has the same equator crossing time of 13:30±10 min as the Suomi National Polar-orbiting Partnership (SNPP) satellite on which the first VIIRS instrument resides, and has the same nominal orbital time period of 101.5 min. Like the SNPP VIIRS instrument, the fourteen VIIRS reflective solar bands (RSBs) with design band central wavelengths from 0.41 to 2.25 μm are radiometrically calibrated on-orbit primarily by observing the onboard sunlit solar diffuser (SD)[1]. The on-orbit change in the SD's bidirectional reflectance distribution function (BRDF) is derived from the ratio of the adjusted signal strengths of the onboard solar diffuser stability monitor (SDSM) at the SD and the sun views, with the sunlight passing through the respective SD and SDSM screens.

Earth Observing Missions and Sensors: Development, Implementation, and Characterization V
edited by Xiaoxiong Xiong, Toshiyoshi Kimura, Proc. of SPIE Vol. 10781, 107810F
 · doi: 10.1117/12.2324529

Both screen transmittances were measured prelaunch, as well as the BRDF[2]. However, previous experience shows that the prelaunch screen transmittances may not be accurate enough to allow for producing a smooth H-factor versus time curve, with the H-factor denoting the on-orbit change of the BRDF[3-6]. Like the case for the SNPP VIIRS[7], yaw maneuvers were performed for the N20 VIIRS to improve the accuracy. Previous experience also shows that the yaw maneuver data alone are not enough to produce accurate SDSM screen relative transmittance and for the SNPP VIIRS some of the regular on-orbit data were used, in addition to the yaw maneuver data, to generate more accurate SDSM screen relative transmittance[5] and the relative product of the SD screen transmittance and the BRDF at the launch time[6]. In this proceeding, we do the same for the N20 VIIRS.

2. SDSM SCREEN RELATIVE TRANSMITTANCE FROM ON-ORBIT DATA

To improve the accuracy of the screens, 15 yaw maneuvers were performed on satellite orbits 972 to 986. In the SDSM screen coordinate system defined in Figure 1(b), the solar angles when the SDSM sees the sun through the SDSM screen are plotted in Figure 1(a). Figure 1(a) shows that the step size along the solar azimuth angle $\phi_{\mathrm{H,SDSM}}$ may be too large to resolve the fine structure associated with the SDSM screen transmittance. Thus, as we did for the SNPP VIIRS SDSM screen[5], we would also like to use regular on-orbit data.

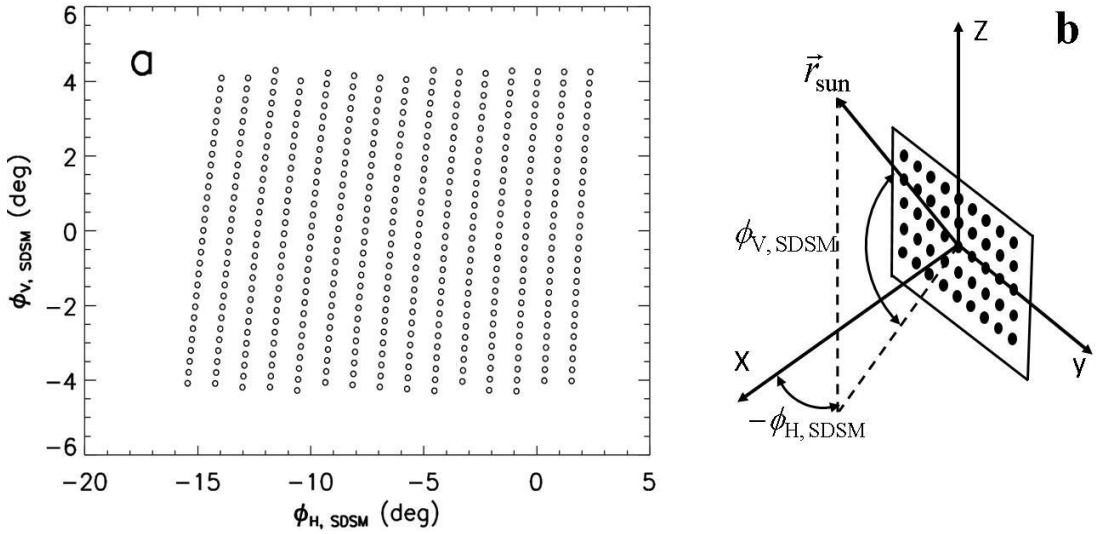

Figure 1. (a) Solar angles for the 15 yaw maneuvers when the SDSM sees the Sun through the SDSM screen, plotted in the SDSM screen coordinate system defined in (b). (b) Definition of the SDSM screen coordinate system. The x axis is along the SDSM screen normal and the z axis is along the short dimension of the screen. $\vec{r}_{\mathrm{sun}}$ indicates the solar vector.

To avoid the adverse effect of the drifts of the SDSM detector gain and the solar spectral power, ideally we would like to use a portion of regular on-orbit data whose solar angles cover the entire range in the mission in the least amount of time. However, up to day 211 since the mission start, we do not have such regular on-orbit data. The solar azimuth angles at $\phi_{\mathrm{V,SDSM}} = 0$ since the mission start are plotted in Figure 2. The regular on-orbit data that we choose are indicated in the figure. To reduce the adverse impact of the drifts of the SDSM detector gains and the solar spectral power, we divide the regular on-orbit data into 9 segments, indicated by the numerical numbers 1-9 in the figure. Each of the regular on-orbit data segments is around one of the yaw maneuvers in terms of the solar angles. In the figure, the pluses are for the yaw maneuvers and the dashed lines indicate the segment boundaries. Note that the dashed lines are not plotted for all regular on-orbit data segments.

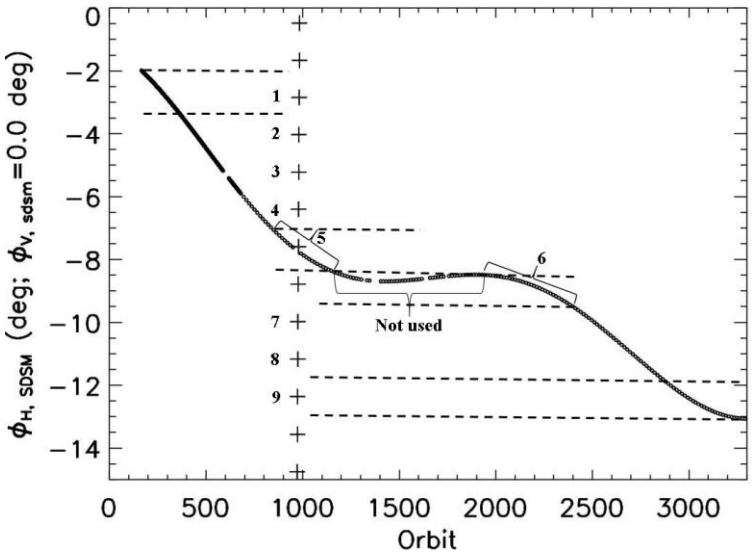

Figure 2. Solar azimuth angles at $\phi_{\mathrm{V,SDSM}} = 0$. The circles and the pluses are for the regular on-orbit and the yaw maneuvers, respectively. The 1-9 indicate the regular on-orbit data segment index. The dashed lines indicate the segment boundaries, not plotted for all regular on-orbit data segments.

We use the following formula to calculate the SDSM screen relative transmittance with on-orbit data that include the yaw maneuver data[5]

$$\frac{\tau_{\mathrm{SDSM,eff}}(\vec{\phi}(t),d)}{\tau_{\mathrm{SDSM,eff}}(\vec{\phi}(t_{\mathrm{mid}}),d)} = \frac{dc_{\mathrm{sun}}(t,d)d^2_{\mathrm{VIIRS-sun}}(t)}{dc_{\mathrm{sun}}(t_{\mathrm{mid}},d)d^2_{\mathrm{VIIRS-sun}}(t_{mid})} \times [1 + c_{1,\mathrm{SDSM}}(t\text{-}t_{\mathrm{mid}}) + c_{2,\mathrm{SDSM}}(t - t_{\mathrm{mid}})^2] , \quad (1)$$

where $\tau_{\mathrm{SDSM,eff}}$ is the effective SDSM screen transmittance for SDSM detector d, $\vec{\phi}$ is the solar angle, dc_{sun} is the digital count with the background subtracted when the sunlight goes through the SDSM screen to hit the detector, $d_{\mathrm{VIIRS-sun}}$ is the distance between the Sun and the VIIRS, and t_{mid} is the time for a data point that is at or close to the middle of the data sequence. The left side of equation (1) is the SDSM screen relative transmittance denoted as $\tau^{\mathrm{R}}_{\mathrm{SDSM,eff}}$. In equation (1), $c_{1,\mathrm{SDSM}}$ and $c_{2,\mathrm{SDSM}}$ are the Taylor polynomial coefficients of

$$\frac{\int_0^\infty d\lambda \times \mathrm{SR}_{\mathrm{SDSM}}(\lambda,t_{\mathrm{mid}},d)\Phi_{\mathrm{sun}}(\lambda,t_{\mathrm{mid}})}{\int_0^\infty d\lambda \times \mathrm{SR}_{\mathrm{SDSM}}(\lambda,t,d)\Phi_{\mathrm{sun}}(\lambda,t)} , \quad (2)$$

where the $\mathrm{SR}_{\mathrm{SDSM}}$ denotes the spectral response of the detector and Φ_{sun} denotes the solar spectral power. For the yaw maneuvers, $t - t_{\mathrm{mid}}$ is small enough to make $| c_{1,\mathrm{SDSM}}\ (t\text{-}t_{\mathrm{mid}}) + c_{2,\mathrm{SDSM}}(t - t_{\mathrm{mid}})^2|$ much less than one and its impact on the relative transmittance negligible. For regular on-orbit data, as we did before, we scale the regular on-orbit data segment determined $\tau^{\mathrm{R}}_{\mathrm{SDSM,eff}}$ to match the yaw maneuver data determined $\tau^{\mathrm{R}}_{\mathrm{SDSM,eff}}$ and then match the values at the segment boundaries to refine the initial value of $c_{1,\mathrm{SDSM}}$. Note the value of expression (2) is from the sun view response with adjustments for the prelaunch $\tau^{\mathrm{R}}_{\mathrm{SDSM,eff}}$ and the VIIRS-Sun distance squared.

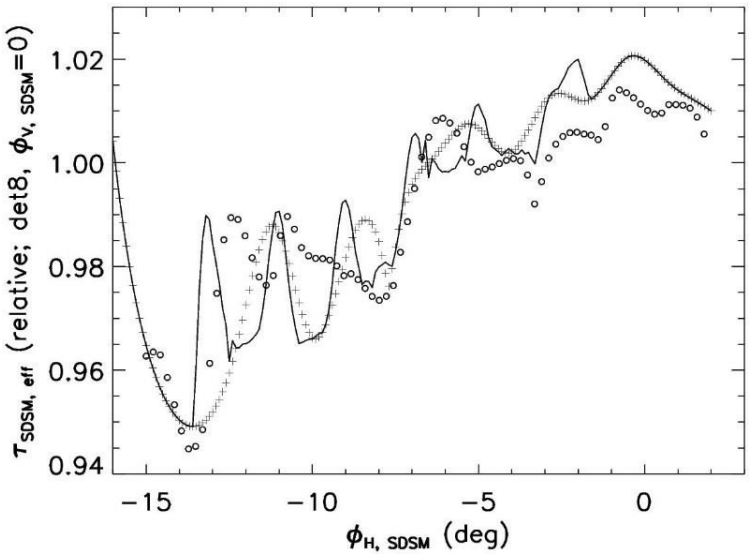

Figure 3. $\tau^{\mathrm{R}}_{\mathrm{SDSM,eff}}$ versus $\phi_{\mathrm{H,SDSM}}$ at $\phi_{\mathrm{V,SDSM}} = 0$ for SDSM detector 8: circles (prelaunch), pluses (yaw maneuvers), and solid line (yaw + regular on-orbit data).

As an example to compare the SDSM screen relative transmittances, in Figure 3 we plot the $\tau^{\mathrm{R}}_{\mathrm{SDSM,eff}}$ versus $\phi_{\mathrm{H,SDSM}}$ for SDSM detector 8 at $\phi_{\mathrm{V,SDSM}} = 0$ from the prelaunch measurements (circles), the yaw maneuvers (pluses), and the yaw maneuvers plus the regular on-orbit data (solid line). The figure shows that the $\tau^{\mathrm{R}}_{\mathrm{SDSM,eff}}$ from the yaw maneuver and regular on-orbit data differs significantly from the yaw maneuvers alone and the prelaunch $\tau^{\mathrm{R}}_{\mathrm{SDSM,eff}}$. In the figure, over the solar azimuth angles covered by segments 2-8, the largest difference between the $\tau^{\mathrm{R}}_{\mathrm{SDSM,eff}}$ from the yaw maneuver data alone and the yaw maneuvers plus regular on-orbit data is around 1.0%. For the boarder segments, segments 1 and 9, the drift rate for the combined SDSM detector gain and solar spectral power may not be accurately known and hence large error may occur for the obtained $\tau^{\mathrm{R}}_{\mathrm{SDSM,eff}}$. However, the same amount of error also occurs for the SD screen and thus cancels out in the H-factor calculation. When $\phi_{\mathrm{H,SDSM}}$ is less than -13.7° or larger than -1.7°, there are no regular on-orbit data thus far in the mission, and over these angular regions we use the yaw maneuver data determined $\tau^{\mathrm{R}}_{\mathrm{SDSM,eff}}$ for the $\tau^{\mathrm{R}}_{\mathrm{SDSM,eff}}$ determined from the yaw maneuvers plus regular on-orbit data.

3. THE RELATIVE PRODUCT OF THE SD SCREEN TRANSMITTANCE AND THE BRDF FROM THE ON-ORBIT DATA

There are two relative products of the SD screen transmittance and the BRDF at the mission start. One is for the RTA SD view and the other for the SDSM SD view, denoted respectively by $\tau^{\mathrm{R}}_{\mathrm{SD}}\mathrm{BRDF}_{\mathrm{RTA}}$ and $\tau^{\mathrm{R}}_{\mathrm{SD}}\mathrm{BRDF}_{\mathrm{SDSM}}$.

$\tau^{\mathrm{R}}_{\mathrm{SD}}\mathrm{BRDF}_{\mathrm{SDSM}}$ is calculated by[6], for a particular SDSM detector *d*,

$$\tau^{\mathrm{R}}_{\mathrm{SD}}\mathrm{BRDF}_{\mathrm{SDSM}}(d) = \frac{dc_{\mathrm{SD}}(t,d)\,d^2_{\mathrm{VIIRS-sun}}(t)\cos\theta_{\mathrm{SD-sun}}(t_{\mathrm{mid}})}{dc_{\mathrm{SD}}(t_{\mathrm{mid}},d)\,d^2_{\mathrm{VIIRS-sun}}(t_{mid})\cos\theta_{\mathrm{SD-sun}}(t)} \times \frac{1+c_{1,\mathrm{SDSM}}(t-t_{\mathrm{mid}})+c_{2,\mathrm{SDSM}}(t-t_{\mathrm{mid}})^2}{1+c_{1,\mathrm{H}}(t-t_{\mathrm{mid}})+c_{2,\mathrm{H}}(t-t_{\mathrm{mid}})^2} \quad , \tag{3}$$

where $c_{1,\mathrm{H}}$ and $c_{2,\mathrm{H}}$ are the quadratic Taylor polynomial coefficients for $\mathrm{H}_{\mathrm{SDSM}}(d,t)/\mathrm{H}_{\mathrm{SDSM}}(d,t=0)$ that is calculated initially with the prelaunch $\tau^{\mathrm{R}}_{\mathrm{SD}}\mathrm{BRDF}_{\mathrm{SDSM}}$, where the $\mathrm{H}_{\mathrm{SDSM}}$ is the H-factor along the SD-to-SDSM direction. $c_{1,\mathrm{H}}$ is

adjusted through matching at the segment boundaries. In equation (3), dc_{SD} is the digital count with the background subtracted when the sunlight reflected off the SD enters the SDSM.

Unlike the case for $\tau^{\mathrm{R}}_{\mathrm{SDSM,eff}}$, when away from the solar azimuth angles that are covered by segments 1 and 9, in the solar azimuth angular range of 14° to 26° in the VIIRS coordinate system (defined in the Figure 4 caption), the on-orbit data determined $\tau^{\mathrm{R}}_{\mathrm{SD}}\mathrm{BRDF}_{\mathrm{SDSM}}$ does not differ much from the prelaunch one, shown by Figure 4, a reflection of the large number of through holes (hundreds) on the SD screen, seen by each SDSM detector.

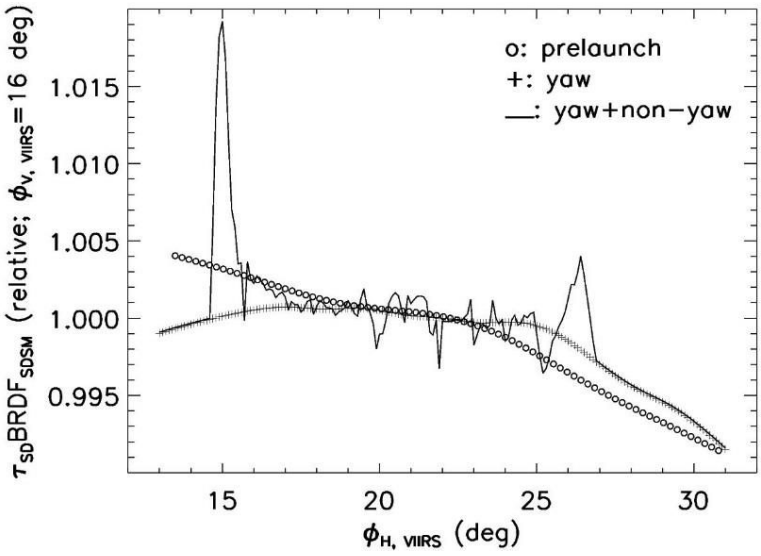

Figure 4. $\tau^{\mathrm{R}}_{\mathrm{SD}}\mathrm{BRDF}_{\mathrm{SDSM}}$ versus $\phi_{\mathrm{H,\ VIIRS}}$ at $\phi_{\mathrm{V,\ VIIRS}} = 16°$ for SDSM detector 8. The VIIRS coordinate system is defined as: the x axis is along the SD screen normal and $\phi_{\mathrm{V,\ VIIRS}}$ is the angle between the solar vector projected onto the xz plane and the x axis, where the z axis is along the short dimension of the SD screen, in the opposite direction of the Earth View port central vector that originates from the rotating telescope assembly.

$\tau^{\mathrm{R}}_{\mathrm{SD}}\mathrm{BRDF}_{\mathrm{RTA}}$ is calculated by[6], for a particular detector *d* in a particular band B,

$$\tau^{\mathrm{R}}_{\mathrm{SD}}\mathrm{BRDF}_{\mathrm{RTA}}(d) = \frac{F(t)P(dn_{\mathrm{SD}}(t))}{F(t_{\mathrm{mid}})P(dn_{\mathrm{SD}}(t_{\mathrm{mid}}))} \times \frac{d^2_{\mathrm{VIIRS-sun}}(t)\cos\theta_{\mathrm{SD-sun}}(t_{\mathrm{mid}})}{d^2_{\mathrm{VIIRS-sun}}(t_{\mathrm{mid}})\cos\theta_{\mathrm{SD-sun}}(t)} \times \frac{1}{1+c_{1,\mathrm{H}}(t-t_{\mathrm{mid}})} \quad . \tag{4}$$

In equation (4), $P(dn_{\mathrm{SD}}) = c_0 + c_1 dn_{\mathrm{SD}} + c_2 dn^2_{\mathrm{SD}}$ where dn_{SD} is the RSB detector digital number with background subtracted, and the c-coefficients are from the prelaunch values. We omit the quadratic term associated with $c_{2,\mathrm{H}}$ since for this product we only want to use the yaw maneuver data that occurred over a very short time duration. In equation (4) the *F* is the F-factor that multiplies $P(dn_{\mathrm{SD}})$ to yield the correct spectral radiance[1], calculated with the prelaunch $\tau_{\mathrm{SD}}\mathrm{BRDF}_{\mathrm{RTA}}$.

$\tau_{\mathrm{SD}}\mathrm{BRDF}_{\mathrm{RTA}}$ is obtained by multiplying a scale factor to the $\tau^{\mathrm{R}}_{\mathrm{SD}}\mathrm{BRDF}_{\mathrm{RTA}}$. The scale factor is found through a least-squares match with the prelaunch $\tau_{\mathrm{SD}}\mathrm{BRDF}_{\mathrm{RTA}}$, over the solar angular range of $\phi_{\mathrm{V,\ VIIRS}} = [14°, 18°]$ and $\phi_{\mathrm{H,\ VIIRS}} = [14°, 30°]$. As an example, Figure 5 compares prelaunch and the yaw maneuver data determined $\tau_{\mathrm{SD}}\mathrm{BRDF}_{\mathrm{RTA}}$ for the M1 band detector 8 with the detector index starting from 1. The figure shows that the difference between the $\tau_{\mathrm{SD}}\mathrm{BRDF}_{\mathrm{RTA}}$ from the prelaunch measurements and the yaw maneuver data is very small over the entire solar angular range with the largest difference magnitude less than 0.3%.

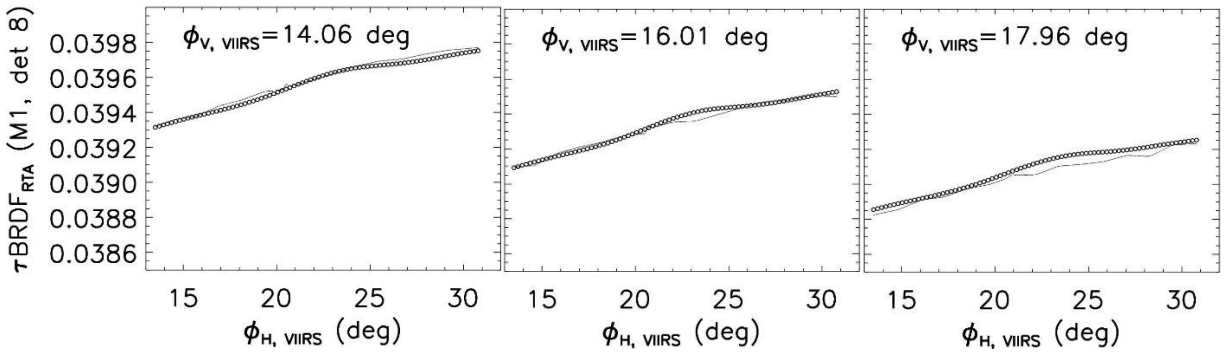

Figure 5. $\tau_{SD}\mathrm{BRDF}_{RTA}$ versus $\phi_{H,\ VIIRS}$ at three $\phi_{V,\ VIIRS}$ for the M1 band detector 8 where the detector index starts from 1: prelaunch (circles) vs. yaw maneuver data determined (solid lines).

4. COMPARISON OF H_{SDSM} FROM THE SCREENS

To evaluate the effectiveness of the $\tau^{R}_{SDSM,eff}$ and $\tau^{R}_{SD}\mathrm{BRDF}_{SDSM}$ that were determined in the previous sections, we compare the retrieved H-factors along the SD-to-SDSM direction, denoted as H_{SDSM}. Figure 6 plots the H_{SDSM} for all eight SDSM detectors, with the left chart for the prelaunch screens, the middle chart for the yaw maneuver data determined screens, and the right chart for the combined yaw maneuver and regular on-orbit data determined screens. The figure shows that the performance of the prelaunch screens is the worst, with the corresponding H_{SDSM} undulates so much that it is difficult to visually see the decrease of the H_{SDSM} for detectors 6-8. The yaw maneuver data determined screens perform much better. The screens from the combined yaw maneuver and regular on-orbit data perform the best with the corresponding H_{SDSM} behaving very smoothly with time, comparable to the smoothness for the derived H_{SDSM} for the SNPP VIIRS[6].

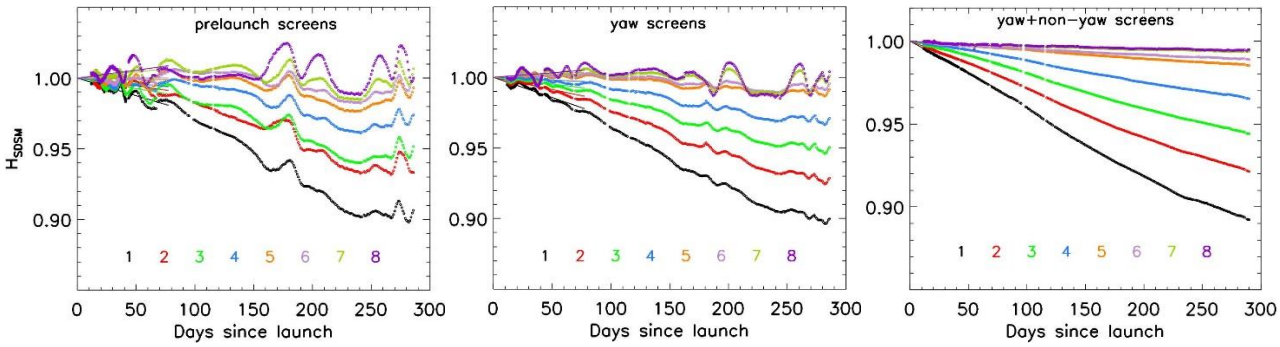

Figure 6. H_{SDSM} derived with (left) prelaunch, (middle) yaw maneuver data, and (right) yaw maneuvers plus regular on-orbit data.

5. SUMMARY

Fifteen yaw maneuvers were performed in the early N20 mission to help derive more accurately the VIIRS SDSM screen relative transmittance $\tau^{R}_{SDSM,eff}$ and the relative products of the SD screen transmittance and the BRDF at the initial time (mission start) $\tau^{R}_{SD}\mathrm{BRDF}_{SDSM}$ and $\tau^{R}_{SD}\mathrm{BRDF}_{RTA}$. The H-factor, that denotes the on-orbit change of the SD BRDF, calculated from the yaw maneuver data determined $\tau^{R}_{SDSM,eff}$ shows large unreal undulations, in particular for SDSM detector 8, exceeding 1%, a result of the large step size in the solar azimuth angles in the yaw maneuvers. To improve the accuracy of the $\tau^{R}_{SDSM,eff}$ and $\tau^{R}_{SD}\mathrm{BRDF}_{SDSM}$, we have used both the yaw maneuver and a portion of regular on-orbit data. As we did

for the SNPP VIIRS screens, to avoid the adverse effect of the drifts in the SDSM detector gain and the solar power, we divide the regular on-orbit data into smaller segments each one of which covers the solar angles of a particular yaw maneuver. We use the yaw maneuver data determined screens as the anchors and scale the regular on-orbit data determined screens to match the anchors. The methodology to derive $\tau^{\mathrm{R}}_{\mathrm{SDSM,eff}}$ for each on-orbit data segment is the same as we did previously whereas the methodology for deriving $\tau^{\mathrm{R}}_{\mathrm{SD}}\mathrm{BRDF}_{\mathrm{SDSM}}$ is similar by treating the SDSM spectral response function as a scaled Dirac delta function. The yaw maneuver and regular on-orbit data determined $\tau^{\mathrm{R}}_{\mathrm{SDSM,eff}}$ differs from the $\tau^{\mathrm{R}}_{\mathrm{SDSM,eff}}$ determined from the yaw maneuver data alone by more than 1% for SDSM detector 8 over some solar angles that are away from that covered by the end regular on-orbit data segments. For the end regular on-orbit data segments, the knowledge in the drifts in the SDSM detector gain and the solar power may not be accurate enough but the impact of the drifts could be small for the calculated H-factor due to cancellation. $\tau^{\mathrm{R}}_{\mathrm{SD}}\mathrm{BRDF}_{\mathrm{SDSM}}$ derived from both the yaw maneuver and regular on-orbit data differs much less than the case for $\tau^{\mathrm{R}}_{\mathrm{SDSM,eff}}$ when away from the solar angles covered by the end regular on-orbit data segments, a reflection of the large number of though holes seen by the SDSM detectors. We have used only yaw maneuver data to calculate $\tau^{\mathrm{R}}_{\mathrm{SD}}\mathrm{BRDF}_{\mathrm{RTA}}$ which is then scaled to match the prelaunch $\tau_{\mathrm{SD}}\mathrm{BRDF}_{\mathrm{RTA}}$. The yaw maneuver data determined $\tau_{\mathrm{SD}}\mathrm{BRDF}_{\mathrm{RTA}}$ differs from the prelaunch one insignificantly, by no more than 0.3% for the M1 band detector 8. The H-factor calculated from the final $\tau^{\mathrm{R}}_{\mathrm{SDSM,eff}}$ and $\tau^{\mathrm{R}}_{\mathrm{SD}}\mathrm{BRDF}_{\mathrm{SDSM}}$ shows significant improvement with the smoothness of the time curve visually matching that for the SNPP VIIRS.

ACKNOWLEDGMENTS

We thank Kevin Twedt of Science Systems and Applications, Inc. (SSAI), Lanham, MD, USA, for many review comments.

REFERENCES

1. Joint Polar Satellite System (JPSS) VIIRS Radiometric Calibration Algorithm Theoretical Basis Document (ATBD); NASA Goddard Space Flight Center: Greenbelt, MD, USA, 2013.

2. H. Oudrari, J. McIntire, X. Xiong, J. Butler, S. Lee, N. Lei, T. Schwarting, and J. Sun, "Prelaunch Radiometric Characterization and Calibration of the S-NPP VIIRS Sensor", *IEEE Trans. Geosci. Remote Sens.*, vol. 53, pp. 2195-2210, 2015, DOI: 10.1109/TGRS.2014.2357678.

3. X. Xiong, J. Butler, W. Barnes, and B. Guenther, "Sensor On-orbit Calibration and Characterization Using Spacecraft Maneuvers", *Proc. IEEE International Geoscience and Remote Sensing Symposium*, pp. 2256-2259, 2007.

4. J. Sun and M. Wang, "On-orbit characterization of the VIIRS solar diffuser and solar diffuser screen", *Applied Optics*, vol. 54, pp. 236-252, 2015.

5. N. Lei, X. Chen, and X. Xiong, "Determination of the SNPP VIIRS SDSM Screen Relative Transmittance from Both Yaw Maneuver and Regular On-Orbit Data", *IEEE Trans. Geosci. Remote Sens.*, vol. 54, pp. 1390-1398, 2016, DOI: 10.1109/TGRS.2015.2480039.

6. N. Lei and X. Xiong, "Products of the SNPP VIIRS SD Screen Transmittance and the SD BRDFs from Both Yaw Maneuver and Regular On-orbit Data", *IEEE Trans. Geosci. Remote Sens.* vol. 55(4), pp. 1975-1987, 2017; DOI: 10.1109/TGRS.2016.2633967.

7. J. McIntire, D. Moyer, B. Efremova, H. Oudrari, and X. Xiong, "On-orbit Characterization of S-NPP VIIRS Transmission Functions", *IEEE Trans. Geosci. Remote Sens.*, vol. 53, pp. 2354-2892, 2015.